ELSEVIER

Journal of Molecular Catalysis A: Chemical 166 (2001) 147–165

JOURNAL OF MOLECULAR CATALYSIS A: CHEMICAL

www.elsevier.com/locate/molcata

Dynamics of benzene in zeolite KL

Carine Hansenne, Fabien Jousse, Laurence Leherte, Daniel P. Vercauteren*

Laboratoire de Physico-Chimie Informatique, Institute for Studies in Interface Sciences, Facultés Universitaires Notre-Dame de la Paix, Rue de Bruxelles 61, B-5000 Namur, Belgium

Received 6 January 2000; received in revised form 25 February 2000; accepted 23 March 2000

Abstract

Zeolites can be viewed as 'solid solvents', wherein an adsorbed molecule is confined within narrow pores and interacts with the zeolite framework and the exchangeable cations. However, it is not clear what part entropy plays in this confinement effect. It is often assumed, especially in cation-containing zeolites, that the entropy effects are negligible, so that all conclusions about adsorption and diffusion are drawn from energetic considerations alone, such as adsorption energies and energy barriers to the diffusion. In order to test this hypothesis, we have undertaken the study of adsorption and dynamics of benzene in zeolite L, with (KL) and without (LTL) compensating K^+ cations. We have constructed and validated against experimental data a model of zeolite KL with Si/Al = 3. Adsorption and dynamics of benzene in this zeolite were studied using static simulation methods, i.e. molecular docking and constrained energy minimization, as well as molecular dynamics (MD) simulations at various temperatures and loadings. All simulations used standard techniques available within MSI's Cerius^2 and InsightII environments. Our simulations show a large discrepancy between the two types of methods, revealing the importance of entropy, even in KL: energy tends to localize adsorption on the cation, entropy to delocalize it over the cage; energy tends to favor adsorption at a 12-membered ring (12T) window between two cages, entropy to destabilize this site; energy tends to cluster up to three benzene molecules within the same cage, entropy to spread the molecules over all cages. From a linear fit with temperature of the free-energy barrier due to the potential of mean-force (MF) along the channel axis, we can estimate an order of magnitude of the entropic barrier to the diffusion through the 12T window as 0.02 kJ mol^{-1} K^{-1} between 200 and 600 K at infinite dilution, both in LTL and KL.

Keywords: Zeolite; Benzene; Simulation; Solvent; Entropy

1. Introduction

A numerous literature concentrates on simulating adsorption and diffusion of molecules in the pores of zeolites: in addition to the industrial interest of predicting the behavior of adsorbates in their cavities and channels [1], diffusion in zeolites appeals to the theoretician and experimentalist alike because of the possibility to study a molecule in a very special environment, where it is confined in narrow pores and feels strong electric effects due to the partly ionic nature of the host framework. The narrowness of the pores, often of a size comparable with the kinetic diameter of the adsorbate, and its special shape or 'corrugation', leads to a sort of solvatation of the adsorbed molecule; this led Derouane to define zeolites as 'solid solvent' [2]. Whereas in proteins solvent effects contain a large entropic part, due to the rearrangement of the solvent around the molecule, in zeolites the framework remains very largely fixed. Therefore it seems difficult to define what the entropic part plays in the confinement effect. For example, Jousse et al. have shown

* Corresponding author.

1381-1169/01/$ – see front matter
PII: S1381-1169(00)00459-3

that the most probable position for butene isomers in the cation-free zeolite silicalite-2, is different from the minimum energy positions [3]. Smit and coworkers proposed that entropic effects can induce separation of branched from linear hydrocarbons in silicalite-1, another cation-free zeolite [4,5]. These examples clearly show the importance of entropic effects, at least in cation-free zeolites. Unfortunately, much less data are available for cation-containing zeolites.

Early molecular dynamics (MD) studies of adsorbed molecules in zeolites already included cations [6,7]. However, these cations may occupy non-periodic positions in the framework, and therefore complicate the interpretation of the data. Furthermore, the interaction between cation and adsorbate is rather stronger than that between adsorbate and the rest of the framework, thus impeding diffusion, so that the estimation of self-diffusion coefficients on manageable computing time becomes very difficult. Therefore, more recent MD studies concentrated on cation-free zeolites, such as silicalite: this simplification allowed to study diffusion coefficients and other long-time effects. Today most MD studies still concentrate on cation-free zeolites [8] with only few exceptions [9], and indeed the self-diffusion coefficient of adsorbed molecules in most cation-containing zeolites still appears out of reach of classical MD [10]. In these cases alternate techniques can be used, such as free-energy sampling [11]. In general, the diffusion mechanism of adsorbed molecules will be different between cation-containing and cation-free zeolites: the strong and localized interactions between extra framework cations resulting in an Arrhenius-like behavior, where diffusion is activated by the thermal fluctuations of the framework, while in absence of such interactions the diffusion is controlled by 'deterministic chaos' [12]. Therefore it appears difficult to infer diffusivities in cation-containing zeolites from the diffusivities observed in their all-siliceous counterparts. In most cases, where cation-containing zeolites are investigated, simple energy minimization techniques are used to locate stable adsorption sites and estimate the diffusion pathway, based on the assumption that in those cases entropic effects are negligible compared with energetic effects [13]. These docking or constrained energy minimization techniques are available in commercial software, such as MSI's Cerius^2 [14] and InsightII packages [15], and routinely used in catalysis to test the effectiveness of a particular zeolite structure.

The energetic part of confinement effects has been studied theoretically by Derouane and coworkers [16,17]. They have shown that a molecule in a narrow pore is more strongly adsorbed when there is a close fit between the size of the molecule and that of the pore. This has also been noted, using MD simulations, by Yashonath and coworkers [18–21] in a series of publications. The importance of the entropic factor remains however unclear; in particular, the assumption that it is relatively unimportant is not proven in the general case. MD simulations, by providing temperature effects and an explicit temperature dependence, can at least partly answer this question, even if we cannot get a reliable average diffusion coefficient in the long-time regime. Indeed, from MD data we can access: (i) the most probable temperature-dependent position; (ii) the free-energy profiles, in the adsorption sites; (iii) the external vibrations and librations of the adsorbate at the adsorption sites. All these data allow us to define, and really quantify, entropic effects.

In this article, we focus on comparing static and dynamics results for a system where entropic effects are expected to be rather large: benzene adsorbed into zeolite KL. This zeolite is composed of heavily corrugated unidirectional channels along *z*: these channels form large periodic cyclindrical cages every $\approx$7.5 Å, separated by circular windows made up of 12 tetrahedral (T) atoms, either Si or Al (12T windows). The potassium form of zeolite KL, with a Si/Al ratio of 3.0, is used as a catalyst support for the aromatization of hexane in benzene [22], this explaining the interest shown in studying experimentally adsorption and diffusion of benzene in this zeolite [23–32]. We are not aware of any theoretical study on this particular system, except for a study of the dynamics of xenon in a cation-free zeolite L [33]: in this article, it was shown that the heavy corrugation of the channel (channel tortuosity) is the cause of interesting entropic effects. More recently, Deka and Vetrivel also studied the energetics of alkylbenzenes, also in a cation-free zeolite L [34]. In order to highlight the influence of the cations, we will study both a model zeolite L with potassium cations (KL) and a zeolite with the same topology but without exchangeable cations (LTL). Thus the aim of this article is threefold: (i) to characterize the dynamics of adsorbed benzene; (ii) to determine, and if pos-

sible to quantify, the influence of entropy on confinement effects for this particular system; (iii) to explore the differences brought by the presence of potassium cations in the zeolite cage.

In Section 2 we present the simulation techniques and forcefields employed to define the zeolite models used in the dynamic study, focusing on the location of the cations so as to reproduce as much as possible experimental data. In Section 3 we present the adsorption and diffusion of benzene in the resulting LTL and KL models, obtained from static techniques, i.e. docking and constrained minimization, and from MD simulations at different temperatures and loadings. Finally we conclude in Section 4.

2. Building of the zeolite model

Adsorption in cation-containing zeolite depends very strongly on the exact location of the extra framework cations [35]. One of the major problems in modeling adsorption in these zeolites is therefore to know the exact position and environment of those cations. Indeed, crystallographic or neutron diffraction studies only provide average occupancies that cannot reflect the microscopic heterogeneity of the cation distribution at the adsorbate scale. The exact environment of a given cation depends on the local distribution of aluminum atoms, but also on the arrangements of all other cations. Neutron diffraction has the advantage over conventional X-ray crystallography, that Si and Al atoms can be distinguished. However, since these atoms are not perfectly ordered, except for Si/Al = 1, neutron diffraction also only qualitatively describes the cation environment.

Our aim in constructing a zeolite KL model is to reproduce as accurately as possible the adsorbate's environment, while keeping the model at a manageable scale. We should therefore build a model that remains simple, while offering a measure of how much the cation sites can be heterogeneous. To achieve this aim, we chose the following procedure. We first defined different possible aluminum distributions in a small model zeolite L, constructed from neutron diffraction data. Then we placed compensating cations at the positions of stable energy in each of the model. Comparison between the models therefore gives a measure of the heterogeneity of the cation distribution. The resulting zeolite models are then minimized with several forcefields, and the corresponding infrared (IR) and XRD spectra are computed and compared with experiments, in order to determine the influence on the forcefield on the local cationic sites.

We used the forcefields UFF and Burchart-UFF (BUFF), available within MSI, and compared the results with the forcefields of van Beest, Kramer, and van Santen (BKS) and of Henson and Auerbach (HA). Universal forcefield (UFF) was originally intended to model all atom types [36]. BUFF consists in a re-parametrization of UFF performed by de Vos Burchart and coworkers, to specifically tackle interactions in zeolites [37]. BKS is a well-known forcefield parametrized against ab initio and experimental data to represent the structure and dynamics of silicate and aluminosilicate frameworks [38,39]. While UFF, BUFF, and BKS consider different atom types for aluminum and silicon in a zeolite framework, HA only considers them as an average 'tetrahedral' atom with an average atomic charge value. Since HA is based on the BKS forcefield, they coincide for all-siliceous zeolites [13,40]. Details on the forcefields used here can be found in the appropriate references, and will not be repeated here.

All simulations involving UFF and BUFF were performed with standard techniques utilizing codes available within the MSI's Cerius^2, namely, the modules cation-locator, IR-Raman, diffraction-crystal, and minimizer. Cation-locator uses an iterative algorithm to place compensating extra framework cations of a chosen nature within the negatively charged zeolite framework [14], by placing each cation in turn at the minimum energy position of the cation-framework and cation–cation interaction grid. This procedure has been pioneered by Newsam et al. for the placing of cations in zeolite 4A [41]. IR-Raman allows to compute the IR spectrum of a given structure, from its Hessian matrix calculated at the minimum energy position. For BKS and HA, we used the DIZZY molecular mechanics and MD simulation program [42] to perform MD simulations and minimization of the KL structure. In that case the IR spectra were computed from the Fourier transform of the dipole autocorrelation function during a 200 ps MD run at 300 K, with a 1 fs time-step. XRD spectra are simulated from the final minimum energy structure using the diffraction-crystal module. Computed spectra are

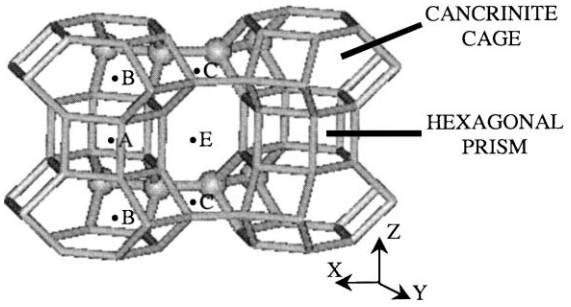

Fig. 1. View at the molecular level of a unit-cell of zeolite L. K^+ cation sites A, B, C, and E are indicated by black dots, T2 atoms by small spheres.

Table 1
Potassium cation positions in zeolite KL, from experimental data of Newsam [25], and determined using the module cation-locator of MSI and subsequent minimization with different forcefields[a]

Cation	Site	Experimental sample	BUFF	UFF	BKS	HA
KA	2 c	−0.01	0	0	0	0
KB	2 d	2.0	2	2	2	2
KC	3 g	3.0	3	3	3	3
KD	6 j	4.76	4	4	3.5	4
KE	3 f	0.16	0	0	0.5	0

[a] Note that the experimental sample contained 10 K^+ cations per unit-cell, while our theoretical model contains only 9.

compared with experimental IR and XRD spectra recorded in-house.

The structure of zeolite L was first determined by Barrer and Villiger in 1969 [43]. Its structure is hexagonal and belongs to the P6/mmm group with unit-cell dimensions $a = b = 18.5$ Å and $c = 7.5$ Å. The framework is built from alternate hexagonal prisms and cancrinite cages, forming large spherical supercages interconnected by 12-membered windows (12T) every ≈7.5 Å along *z*. The chemical composition of one unit-cell of dehydrated KL is $K_9Al_9Si_{27}O_{72}$. Cations have been shown to occupy four types of sites in the hydrated potassium form KL [25,43], as presented in Fig. 1: the A site, localized in the center of the hexagonal prisms, coordinated to six framework oxygens; the B site, located in the center of the cancrinite cages, and coordinated to 12 framework oxygen atoms; the C site, between two cancrinite cages, also coordinated to 12 framework oxygens; and the E site, located in the plane of a 12T window between two supercages, where it is coordinated to six framework oxygens and two water molecules. By dehydration, cations from site E migrate to site D, between two hexagonal prisms. It is noted that there can be some confusion about sites E and D, some authors calling sites D the cations in the 12T window, and E the cations between two hexagonal prisms [27,29]. Since our model zeolite L is based on the neutron diffraction data of Newsam [25], we use here the same nomenclature as used by him.

There are only two non-equivalent T sites in zeolite L: T1 and T2. T2 all are located on the 12T window, while T1 atoms build the rest of the framework (Fig. 1). Neutron diffraction has evidenced that Al atoms preferentially occupy T2 positions in the 12T window [25]. Combined with Lowenstein's rule, this allows to place univocally six of the nine Al atoms within one unit-cell, the remaining three Al occupying T1 sites. This leaves nevertheless 120 possible models, too large a number to be exhaustively explored. Therefore, we built only four different models, chosen so as to represent the different possible Al positioning at the T1 sites. The module cation-locator together with the BUFF forcefield were then used to determine the cation distribution in the resulting models. The corresponding distribution is given in Table 1, under the name BUFF: no difference between the various models is made in this table, because all models resulted in the same distribution, in very good agreement with experimental data. Sites B and C are completely filled, while site A is empty. We note a slight difference in the occupation of sites D and E, that can be attributed to the fact that the experimental KL zeolites contained almost 10 K^+ per unit-cell, while the models used here contain only 9 K^+. Since all models lead to the same cation distribution, we expect them to be equivalent as far as adsorption of benzene is concerned. Therefore we chose arbitrarily one of the models, to be used in the rest of the study.

As can be seen from Table 1, a subsequent minimization with the BUFF, UFF, or HA forcefields does not change the occupancy of the different cationic sites. On the other hand, we note the migration of some cations from a D site to an E site with the BKS forcefield. This migration is caused by the local arrangement of the Al atoms, since the K^+ cations migrate to an E site just above an Al atom. Since with HA

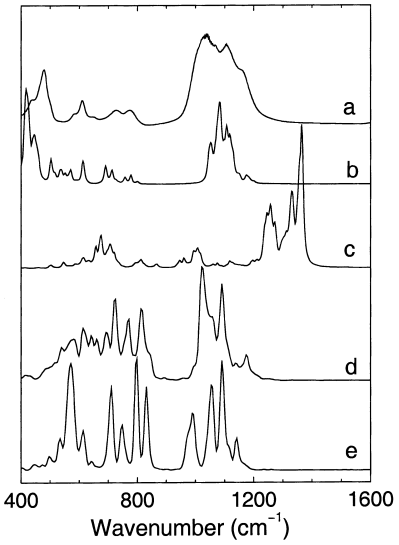

Fig. 2. Experimental and computed IR spectra of zeolite KL with different forcefields and the module IR-Raman of MSI: (a) experimental spectrum; (b) BUFF; (c) UFF; (d) BKS; (e) HA.

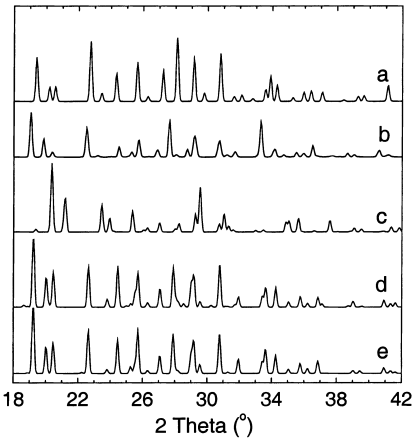

Fig. 3. Experimental and computed XRD spectra of zeolite KL in the medium angle range, using different forcefields and the module diffraction-crystal of MSI: (a) experimental spectrum; (b) BUFF; (c) UFF; (d) BKS; (e) HA.

all T-atoms are equivalent, this migration is not observed. In comparison to experiment, it is quite difficult to assert that the cation distribution obtained using BKS is any better or worse than that obtained using the other forcefields: indeed, site E is also occupied experimentally, although less than what is predicted with BKS.

Figs. 2 and 3 present the IR and XRD spectra in the medium angle region of an experimental hydrated KL zeolite, respectively, as well as the computed spectra using the forcefields UFF, BUFF, HA, and BKS. We can see that BUFF reproduces very well the dynamics of KL both in the T–O stretching region around 1100 cm^{-1} and between 400 and 800 cm^{-1}. HA and BKS also perform quite well in the stretching region, but the agreement worsens toward low frequencies. UFF overestimates all frequencies. The medium angle region XRD spectra shows a very good agreement with the HA and BKS forcefields, and a fair agreement with BUFF. Here again, UFF disagrees completely with experiment. The bad agreement between UFF and experiment, both for structure and frequencies, can be understood by the increase of the unit-cell size by almost 1 Å after minimization of KL with this forcefield. It is clear from the above study that only UFF should be rejected, as it cannot properly model the zeolite structure and dynamics. The three other forcefields BUFF, HA, and BKS, on the other hand, give results in good general agreement with experiment. In what follows, we chose to work with the zeolite KL model minimized using the BUFF forcefield.

3. Adsorption and dynamics of benzene in LTL and KL

The zeolite model constructed in Section 2 is used to study the adsorption and dynamics of adsorbed benzene. We focus in this section on the comparison of results obtained using static simulations methods to those of MD calculations. All simulations were performed with a 18.5 Å × 18.5 Å × 15.0 Å zeolite model, representing one unit-cell along x and y and two unit-cells, corresponding to two cages, along z. Rather than the BUFF forcefield used to describe the framework structure in the above section, we employed the CVFF_AUG forcefield to represent the interaction between the framework and adsorbed molecules: based on the standard CVFF forcefield; it includes a special parametrization for the interaction between zeolite atoms or cations and adsorbed hydrocarbons. In all cases, we fixed the zeolite framework atoms as well as the potassium cations. The calculations were run with full periodic boundary conditions.

We define here static simulation methods as techniques for which there is no explicit temperature dependence, thereby excluding Monte Carlo or similar methods. We employed the standard solid-docking, packing, and constrained energy minimization solid-diffusion procedures available in MSI's InsightII environment. Note that these methods can include some type of statistical information, for example, molecular docking provides a number of minimum energy position that can be analyzed. Both solid-docking and packing modules are based on the same idea: a molecule is randomly inserted into the structure at a position of 'not-too-high' energy, and subsequently minimized. In the docking procedure, a single guest molecule is inserted, while in the packing procedure, several molecules are inserted one after the other. Docking therefore provides the minimum energy sites for a single guest, which can be identified at 0 K with stable adsorption sites, and packing the same results for multiple guests. In both cases, we performed 100 random insertions followed by guest minimization to sample all possible minimum energy sites. The constrained minimization procedure solid-diffusion is used to find out the minimum energy path (MEP) in the structure: the guest molecule's center-of-mass (COM) is constrained to remain in a plane perpendicular to a predefined path in the zeolite framework, usually between stable adsorption sites. At stated intervals along the path, the molecule's energy is minimized, thus allowing to evaluate energy barriers between the stable sites.

Molecular dynamics simulations were performed at different temperatures and loadings. The system was first minimized, and then equilibrated for 10 ps in the NVT ensemble with direct velocity scaling to achieve the desired temperature. The production run consisted of 100–400 ps MD with a 1 fs time-step, in the NVE ensemble; the position and velocity of the guest's COM were saved to file every five steps for subsequent analysis. Dynamics of benzene in zeolite L can be characterized by two kinds of data, differing in nature: average quantities, and frequency-dependent quantities. Average quantities consisted of mean-square displacement (MSD), which is the second moment of the propagator [44].

$$\langle \boldsymbol{r}^2(t)\rangle = \langle |\boldsymbol{r}(t) - \boldsymbol{r}(0)|^2\rangle \tag{1}$$

where $\boldsymbol{r}$ denotes the guest's COM position; the density profile $\rho(z)$ along the channel axis.

$$\rho(z) = \langle \delta[z(t) - z]\rangle \tag{2}$$

where δ is the standard Dirac function. From this density profile we define the potential of mean-force (MF) along the channel axis, sometimes also called the 'constrained free energy' $F(z)$ [45].

$$F(z) = -k_{\mathrm{B}}T \log(\rho(z)) \tag{3}$$

where k_{B} indicates Boltzmann's constant and T the temperature. Note that in the following we will use equivalently the names 'potential of mean-force' or 'free energy', meaning in both case the same quantity defined by Eq. (3). Finally, we computed the pair distribution functions, similar to the density profile $\rho(z)$ but pertaining to the distance between two centers A and B; these are either the COM of two benzene molecules, or the COM of one benzene and a K^+ cation.

$$\rho_{\mathrm{AB}}(z) = \langle \delta[d_{\mathrm{AB}}(t) - z]\rangle \tag{4}$$

The only frequency-dependent quantity we computed consisted of the vibrational density-of-states $G(\sigma)$ (DOS), which is the Fourier transform of the velocity autocorrelation function of the benzene molecule's COM.

$$G(\sigma) = \int \mathrm{d}t \frac{\langle \boldsymbol{v}(t)\boldsymbol{v}(0)\rangle}{\langle \boldsymbol{v}(0)\boldsymbol{v}(0)\rangle} \exp(i2\pi c\sigma t) \tag{5}$$

where $\boldsymbol{v}$ denotes the guest's COM velocity, σ the wavenumber in cm^{-1} and c the velocity of light. $G(\sigma)$ characterizes the external vibrations of the adsorbed molecule within the zeolite channel [46]. Since all runs were performed in the NVE ensemble, the actual temperature of a MD simulation is the average over the production run and therefore might be different from the initial chosen temperature, especially for a single adsorbate, where there are only a few degrees of freedom. We equilibrated MD runs at 200, 300, 400, 500 and 600 K, for one, two and four molecules of benzene in the two unit-cells models of LTL and KL.

3.1. Static results

Docking of a single molecule of benzene in LTL and KL gives very simple results: only one favorable

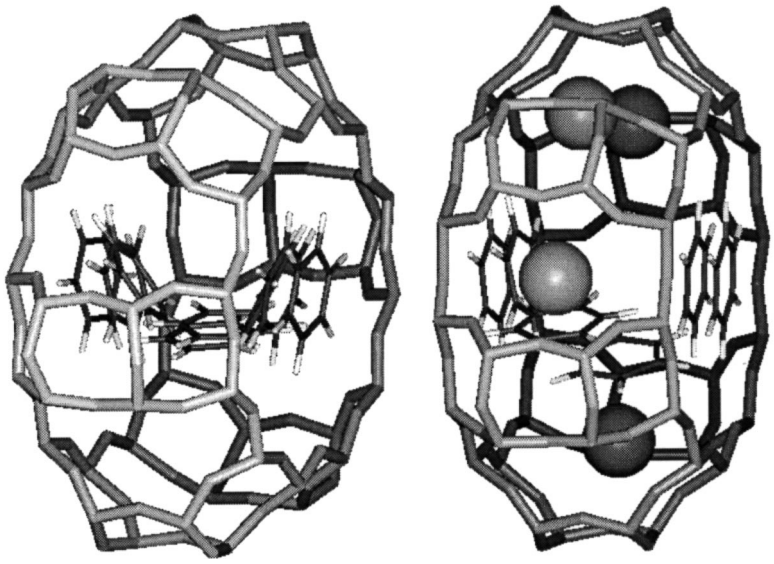

Fig. 4. Minimum energy path of benzene through a cage of zeolites LTL (left) and KL (right), as determined by a constrained minimization procedure using the CVFF_AUG forcefield and the solid-diffusion procedure of MSI. In KL, large balls represent the K^+ cations.

position is found in LTL, where the molecule lies against the zeolite wall (middle position in Fig. 4). In KL on the other hand, there are several stable minimum energy positions (see Fig. 6), that can be put into six different energetic classes. The five lowest energy classes all correspond to the adsorption of the benzene molecule facially on a cation: the cation–COM distance varies between 2.84 and 3.36 Å, without any direct correlation between distance and energy. The type of site corresponds to what has been experimentally measured [23,26], and the distances are close to the experimental distance given in reference [25]: 3.14 Å. The energy difference between the least and most stable member of the class reaches 20 kJ mol^{-1} showing a very broad energy distribution in spite of the simple zeolite model.

The last and least stable class corresponds to benzene adsorbed on a 12T window, in a position close to what is observed in NaY [13,47,48]. The energy lies at ≈22 kJ mol^{-1} higher than that of the most stable sites. It is worth noting that this position is not found in the model LTL used here, most probably because the size of the LTL 12T windows, directly set from neutron diffraction data [25], is slightly smaller than that of the minimized model of KL: 10.4 Å in LTL versus 10.7 Å in KL.

Fig. 4 presents the MEP between two windows of benzene in LTL (left) and KL (right). The corresponding energy profiles are presented in Fig. 5. In LTL, the 12T window corresponds to an energy maximum. The molecule reorients out of the window, so as to face the zeolite wall inside the cage at the minimum energy position. The energy barrier only reaches 7.5 kJ mol^{-1}. The situation is rather different in KL: indeed, the 12T windows constitute local energy minima, appro-

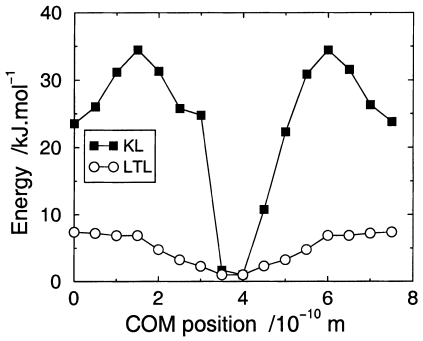

Fig. 5. Energy profile along the MEP of the benzene COM in zeolites LTL and XL, as determined by a constrained minimization procedure using the CVFF_AUG forcefield and the solid-diffusion procedure of MSI. The center of the graph corresponds to the cage and each side to a 12T window.

ximately 10 kJ mol^{-1} below the energy maximum observed along the path. The energy profile, as well as the MEP of Fig. 4, are no longer symmetric with respect to the cage center, due to the heterogeneity of the cation and aluminum positions. The global minimum energy position corresponds to benzene adsorbed facially onto a cation inside the cage. The energy barrier to jump out of this site reaches more than 34 kJ mol^{-1}.

The difference observed between KL and LTL can be explained by two facts: the presence of cations in KL, and the larger size of the 12T window in this zeolite, as compared with LTL. As expected for a cationic zeolite, where the electrostatic interaction with the cations is much larger than with the rest of the zeolite framework, stable energy positions appear to be energetically more stable than in LTL; the corresponding energy barriers are larger: 34 kJ mol^{-1} in KL versus 7.5 kJ mol^{-1} in LTL. The presence of a stable local energy minimum in the 12T window of KL but not in LTL is most probably due to their slightly larger size in KL. This minimum indicates the possibility of stable adsorption onto the windows in KL, which is not observed experimentally [27,31].

The lower part of Fig. 6 presents the energy occurrence $p(E)$ observed by the analysis of a 100 configurations of one, two and four benzene molecules in two unit-cells of KL; on the upper part of the same figure we present, for comparison, the energy occurrence for one and two molecules of benzene in LTL. All energies have been shifted so that the minimum energy of each type is zero. $p(E)$ corresponds to the probability that a given energy is observed as a result of a docking or packing calculation. For all cases, we observe in Fig. 6 a clear bimodal distribution, with a first peak around 3–4 kJ mol^{-1} and a second peak increasing from ≈20 kJ mol^{-1} for one molecule to ≈28 kJ mol^{-1} for two molecules and ≈34 kJ mol^{-1} for four molecules.

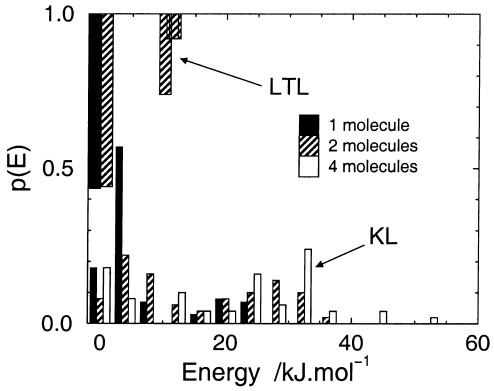

Fig. 6. Top: distribution of the potential energies of one and two molecules of benzene in two unit-cells of zeolite LTL; bottom: distribution of the potential energies of one, two and four molecules of benzene in two unit-cells of zeolite KL, as calculated using MSI's solid-docking and packing procedures with the CVFF_AUG forcefield.

We have seen in the above paragraph that the first five bars, in the case of a single molecule, correspond to benzene adsorbed onto a cation, while the sixth bar corresponds to benzene in the 12T window. The bimodal distribution reflects the same energy ranking, as the lowest peak in all cases is made of benzene exclusively adsorbed onto cations, while the second peak presents one or more molecules adsorbed onto a window. Inside each mode, the broad distribution of the interaction energies reflects two causes: (i) the broad energy distribution of the 'cation site', already observed with only one molecule adsorbed and (ii) the distribution of the favorable benzene–benzene interaction energies. In the two molecule case, most favorable energies within the first peak correspond to two molecules adsorbed on cations in the same cage, while less favorable energies in the first peak correspond to benzene adsorbed onto cations in different cages. In the four molecule case, the most favorable energies correspond to a 3–1 distribution, with three molecules in one cage and only one in the other. This distribution is however very sparsely represented, and all other favorable energies correspond to 2–2 distributions.

The number of configurations with benzene adsorbed onto a window increases when increasing the number of molecules, although these configurations remain energetically less favorable. This suggests that the probability of finding a molecule at a window would increase when increasing the loading, contrarily to what is observed experimentally by IR spectroscopy [31,32].

3.2. Dynamic results

In the course of the data analysis we have noted a particularly interesting phenomenon: after the equilibration period, the total system temperature stabilizes around an average temperature for all runs at all

temperatures, without any subsequent drift. We can separate this temperature into two components, i.e. an internal temperature corresponding to the kinetic energy contained within the internal vibrations of the adsorbate, and an external or 'translational' temperature corresponding to the external vibrations of the adsorbed molecule. In the case of a single benzene molecule adsorbed in KL, we have noted that at the end of the equilibration run the translational temperature is very high, and that it takes the initial 100 ps of the subsequent production run for the external temperature to equilibrate with the internal temperature. Consequently, these initial 100 ps were removed from the analysis of the production run. Curiously, this effect was only observed for the diffusion of a single molecule of benzene in KL, and not for several molecules in the same zeolite, nor for a single benzene in LTL. This observation is especially astonishing, as we have shown in a recent study on a similar system, i.e. benzene adsorbed in NaY zeolite, but with a different forcefield, that energy redistribution in the internal degrees of freedom is quite quicker than what is observed here: less than 20 ps at 100 K [49]. The perversity of this behavior lies in the fact that monitoring the total temperature of the system does not reveal this absence of equilibration. We have found, however, that a simple characteristic signature indicating this behavior can be observed by plotting the average potential energy $\langle U \rangle$ as a function of temperature. Indeed, the equipartition theorem states that $\langle U \rangle = \langle U_0 \rangle + 1/2nk_BT$, where k_B is Boltzmann's constant and n the number of degrees of freedom, which is close to three times the number of atoms for an adsorbed molecule. Non-equilibrated behavior, such as the one we have met, however, do not obey the equipartition theorem, so that the slope of $\langle U \rangle$ as a function of T is very different from the theoretical expectation.

For all temperature studied, and for both model zeolites LTL and KL, the diffusion of benzene appears as a jump diffusion process between the cages. This behavior was expected, since all recent MD studies of adsorbed molecules in zeolites revealed a similar jump process, with the molecule vibrating inside a cage before going to another cage [3,46,50–55].

Fig. 7 presents the potential of MF along one zeolite channel at 500 K, for both LTL and KL, when a single benzene molecule is adsorbed. This potential of MF should be compared with the MEP displayed in Fig. 5, which represents the same quantity at 0 K. For benzene in LTL, the MF profile at 500 K remains rather close to the MEP, although much sharper next to the window; the free energy barrier at 500 K reaches about 10.5 kJ mol^{-1}, which is only slightly larger than the corresponding energy barrier at 0 K: 7.5 kJ mol^{-1}. For KL on the other hand, the profiles are very different: the free-energy barrier is noticeably lower at 500 K than the energy barrier at 0 K: 20 kJ mol^{-1} versus 34 kJ mol^{-1}. Furthermore, there is no longer any local minimum at the 12T window: this site is destabilized by entropy. This entropic destabilization appears quite clearly both for LTL and KL when comparing Fig. 7 with Fig. 5, by the sharpening of the energy profile next to the window for LTL, and by the filling of the energy curve next to the window for KL. This observation remains true for all temperatures studied, from 200 to 600 K, and also for all loading, from one to four molecules per two unit-cells, showing the absence of any stable window site for those temperatures over most of the loading range. A number of runs at high loading were initialized with a molecule in the window, and always resulted by a desorption of this molecule out of the window. Entropic destabilization of the window site is not unexpected, since the volume accessible to the sorbate is much smaller in the window than in the cage. However, that it remains so even at low temperature and high loading is more astonishing, and contradicts the results from the packing study presented in Section 3.1.

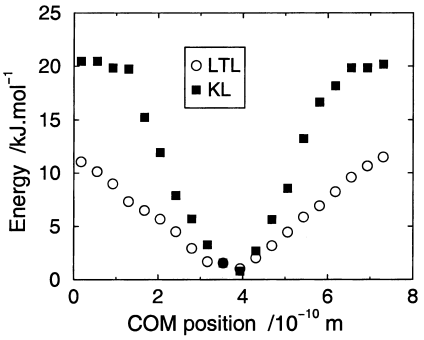

Fig. 7. Potential of MF along the channel axis of zeolites LTL and KL, as computed from 0.4 ns MD at 500 K using CVFF_AUG. As in Fig. 5, the center of the graph corresponds to the cage and each side to a 12T window.

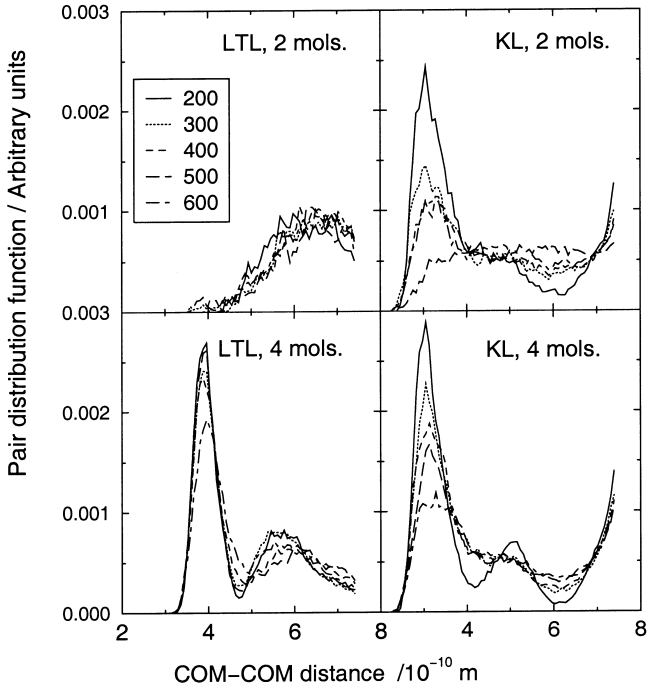

Fig. 8. Pair distribution function $\rho_{AB}(z)$ between the COM of two benzene molecules in zeolites LTL and KL, as computed from 0.1 to 0.4 ns MD using CVFF_AUG at different temperatures and loadings.

Fig. 8 presents the calculated benzene–benzene pair distribution functions (PDF) for all temperatures, in LTL and KL, for two and four molecules per two unit-cells. For two molecules in LTL, the PDFs are basically temperature-independent, and show that the two molecules always occupy separate cages. For four molecules per two unit-cells, the PDFs remain also temperature-independent, but this time present a sharp peak at 4 Å, corresponding to two benzenes in a stable parallel position inside the same cage, and a smaller peak around 6 Å, corresponding to a perpendicular position also inside the same cage. These distances are close to the equilibrium benzene–benzene distances in the dimer [56,57]. That these profiles remain mostly temperature-independent indicates that between 200 and 600 K only entropic effects govern the PDFs: indeed energetic effects would depend exponentially on temperature. By contrast, there is a clear temperature dependence observed in KL. For two molecules, the PDF is made of a sharp peak at low temperature, indicating that the two molecules stay most of the time in the same cage. As the temperature increases, this peak decreases and vanishes completely at 600 K, where two molecules occupy two different cages. For four molecules, the PDFs are also temperature-dependent: at low temperature, two molecules in the same cage tend to adsorb on well-defined cation sites, resulting in two sharp peaks at 3 and 5 Å. These distances are much smaller than for four molecules in LTL, indicating that they are due to cation–benzene interactions rather than benzene–benzene interactions. As the temperature increases, the peaks decrease, showing that the molecules now average their motions over the whole cage.

Free energy profiles as well as benzene–benzene PDFs clearly show the influence of entropic effects affecting the dynamics of benzene in zeolite L. Indeed, entropic effects are preponderant in LTL, where the results completely contradict the packing study mentioned above: at medium loading, benzene molecules occupy different cages, while for high loading, the PDFs show a bimodal distribution close to that of the free benzene dimer. For KL, the window site observed in the solid-docking and packing study vanishes, for

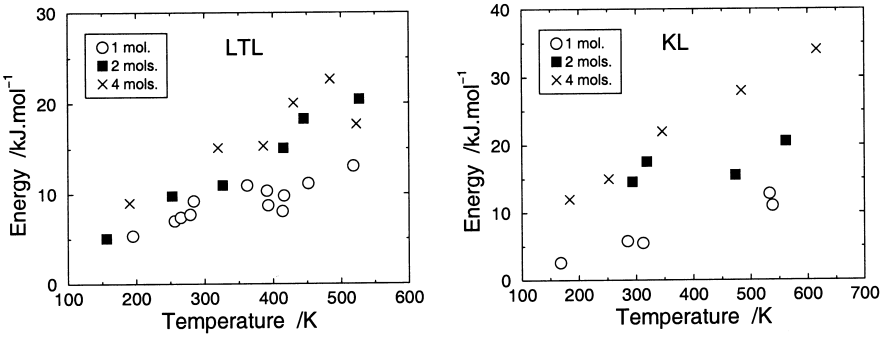

Fig. 9. Temperature dependence of the apparent free energy barriers for different loadings of benzene along the channel of zeolites LTL (left) and KL (right), as computed from 0.1 to 0.4 ns MD using CVFF_AUG.

all loadings and temperatures. The PDFs however depend on temperature, showing a competition between energy and entropy: for two molecules at low temperature, they are located in the same cage, in accordance with the packing results; while at high temperature, they occupy different cages.

We can try to quantify these entropic effects by plotting the temperature dependence of the free energy barriers $F_{\max} - F_{\min}$. While this barrier is very well defined at infinite dilution and high temperature from the simulations, for higher loadings and low temperatures there is a large statistical uncertainty associated with the window region, that nevertheless allows us to estimate an order of magnitude of the free energy barriers. Fig. 9 presents these barriers as a function of temperature, for all temperatures and loadings. Writing $\Delta F = \Delta U - T\Delta S$, ΔU and ΔS can be evaluated from a linear regression of ΔF as a function of T. The corresponding values are given in Table 2. It is rather difficult to estimate the uncertainty on these values: any deviation from a strict linear behavior leads to large errors in the regression, and clearly such errors are expected. Therefore the errors indicated in Table 2, which are purely statistical errors from the linear regression, should be taken only as indicative. In particular, the 'energy barriers' ΔU obtained from this linear regression suffer at least 100% uncertainty. The entropy barriers seem a little better defined. One should first note that they are always negative, indicating that $S^{\ddagger} < S_i$, i.e. the entropy at the transition state is always smaller than in the initial state. This is understandable enough, as the transition state in all cases is the 12T window, where much less space is available to the adsorbed molecule than in the cage. ΔS is similar in this case for both LTL and KL, probably reflecting the available volume, similar with or without cations. For medium loading, the difference between LTL and KL becomes pronounced, as ΔS decreases slightly for KL but increases strongly for LTL. This should be connected with the previous observation, that two molecules tend to occupy the same cage in KL but different cages in LTL: two molecules in the same cage will facilitate cage-to-cage transport by decreasing the available volume inside the cage,

Table 2
Apparent entropy barrier ΔS (kJ mol^{-1} K^{-1}) and energy barrier ΔU (kJ mol^{-1}) for different loadings of benzene in zeolites LTL and KL, as determined from a linear fit of the free energy barriers $\Delta F = \Delta U - T\Delta S$ from Fig. 9[a]

Zeolite	ΔS^{b}	ΔU^{b}	ΔS^{c}	ΔU^{c}	ΔS^{d}	ΔU^{d}
LTL	−0.019 (4)	2.3 (1.3)	−0.042 (3)	−1.5 (1.2)	−0.034 (10)	3.4 (3.9)
KL	−0.025 (3)	−1.8 (1.1)	−0.014 (11)	11.3 (4.6)	−0.052 (3)	2.8 (1.2)

[a] Values in parentheses are estimated standard errors.
[b] One molecule per two unit-cells.
[c] Two molecules per two unit-cells.
[d] Four molecules per two unit-cells.

while in different cages they block each other. For four molecules per two unit-cells, the two effects are present: for LTL the resulting effect is a small decrease of ΔS as compared with medium loading, whereas for KL, the net effect is a large increase of ΔS as compared with medium loading. Another interesting fact is that ΔU obtained from this regression is much lower than what has been measured by solid-diffusion, even taking into account the large uncertainty on ΔU. This is especially true for KL, where the apparent energy barrier at infinite dilution taken from Table 2 is negative, instead of $+34\,\mathrm{kJ\,mol^{-1}}$ observed in Fig. 5. This suggests that, for very low temperatures (less than 200 K), the free energy barriers to the diffusion through the window would decrease with increasing temperature, so that we would have $S^{\ddagger} < S_i$. For low temperatures, where the external motions of the adsorbate are reduced, the fact that the available volume at the window is smaller than in the cage might indeed be less important than for the higher temperatures studied here. In that case a second effect might come into play, described by Henson et al. as the 'tortuosity' of the zeolite L channels [33]. Indeed, the MEP presented in Fig. 4 shows that diffusion of benzene at 0 K through a cage of zeolite L is quite a complex process, involving a reorientation of the molecule from a position parallel to the channel wall, to a position where it is framed in the 12T window. This complex motion will be made easier as temperature increases, resulting in an entropic favoring of the window: in a preceding study of the diffusion of benzene in zeolite NaY, presenting stable adsorption sites next to cations and on 12T windows similar to the those separating the cages of LTL and KL, Jousse and Auerbach [11] have found that the windows are entropically favored over the cage interior, by a factor of five to six at low temperature increasing up to 9 at 800 K. This type of favoring is also probably present in the systems studied here.

Another average quantity of interest to elucidate the behavior of benzene in KL is the cation–benzene COM PDF displayed in Fig. 10 for all temperatures and loadings. For low loading and low temperature, there is a small peak at ≈3.5 Å corresponding to adsorption on a cation; when the temperature increases, this peak vanishes as the molecule samples a larger part of the cage. We note a similar behavior for all loadings, but with sharper peaks for high loading since

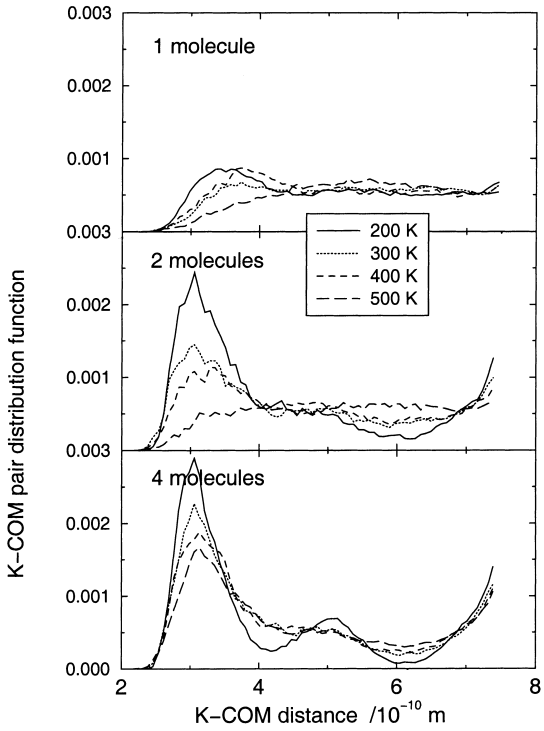

Fig. 10. Cation–benzene COM pair distribution function in zeolite KL, as computed from 0.1 to 0.4 ns MD using CVFF_AUG for different loadings of benzene. Note the scale is the same for all graphs.

the volume available to a single molecule decreases as the loading increases. The peaks are displaced toward lower distances, i.e. ≈3 Å due to the benzene–benzene constraints. These results indicate that adsorption on a cation is only well-defined at low temperatures, or very high loadings. This again mitigates the results of the static solid-docking and packing studies, where only cation adsorption sites were observed. The average cation–benzene COM distance remains comparable with the experimental observation: 3.14 Å [25]. In contrast to the packing study, this average distance decreases with increasing loading, while at 0 K it remains largely fixed.

Since at low temperature or high loading we can define a 'cation adsorption site', such as it is found for example in NaY [11], we can also determine the average residence time at the cation. From Fig. 10, we see that this cation site can be defined if the benzene's COM is less than ≈4.3 Å from the cation.

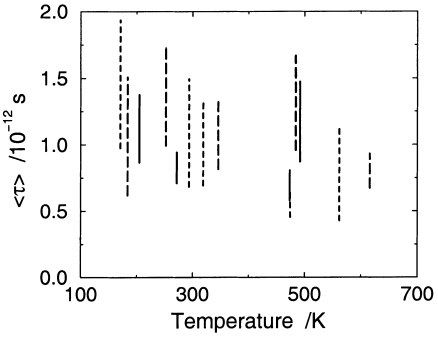

Fig. 11. Average residence time at a cation site, as computed from 0.1 to 0.4 ns MD of benzene at various loadings in zeolite KL using CVFF_AUG. Vertical bars represent the 95% confidence interval. Solid lines: one molecule; dotted lines: two molecules; dashed lines: four molecules.

From this definition we can extract residence times at the cation, presented in Fig. 11. Vertical lines are estimated error bars giving a 95% confidence interval. These error bars are quite large due to a large statistical uncertainty. The main conclusion of this graph is that residence times at cation sites are only weakly dependent on temperature and loading, and vary only between 0.5 and 1.8 ps. In a recent NMR study of benzene in KL, Sato et al. [30] have found a much longer residence time at cation sites, reaching 10^{-6} s at 373 K, and a much larger temperature dependence of these times, corresponding to an activation energy of 18 kJ mol^{-1}. The discrepancy between our simulation results and these experiments reaches six orders of magnitude. The obvious explanation would be that the present simulation results do not represent correctly adsorption at a cation: indeed, we have seen that the cation–framework and cation–benzene distances are overestimated in our simulations, which would lead to a somewhat smaller electrostatic interaction between the cation and the quadrupole of benzene. We do not think, however, that this slight overestimation would lead to differences of such magnitude.

We now turn to frequency-dependent processes. The maximum observable frequency and minimum resolution are proportional to the inverse of the simulation time and sampling frequency, respectively. Although internal vibrations can provide some information about the surrounding of the molecule in its adsorption site [27], we are more interested in molecular motions, such as external vibrations and librations, generally characterized by low frequency (LF) vibrations [58]. Fig. 12 presents the LF spectrum $G(\sigma)$ computed from Eq. (5) at 300 K for benzene in LTL (left) and KL (right). In LTL, $G(\sigma)$ is made of a single band peaked around 18 cm^{-1}, stemming mainly from contributions from *x*- and *y*-axes; those contributions are identical, since the zeolite is symmetric along *x* and *y*. This peak shifts slightly with temperature, from about 12 cm^{-1} at 200 K to 25 cm^{-1} at 600 K: it originates in the vibrations of benzene through the cage, with a frequency roughly proportional to its velocity: $\nu \approx v/l$, where *v* is the COM velocity and *l* the cage length. $G_z(\sigma)$ presents a non-zero contribution at $\sigma = 0$, representing the diffusion along the channel. In KL, we recognize the same peaks, at about the same frequencies along *x* and *y*. However, their 'tail'

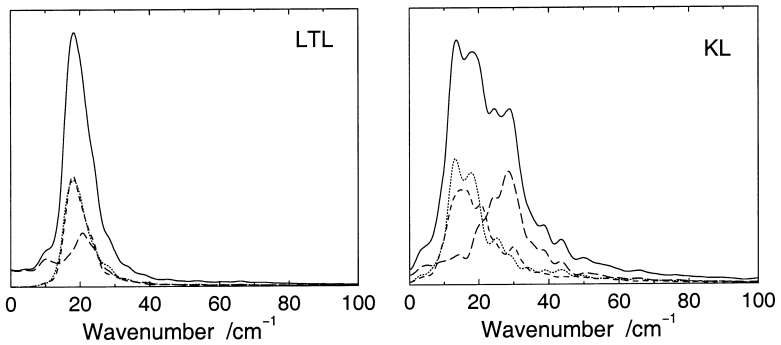

Fig. 12. Vibrational density-of-state $G(\sigma)$ for a single molecule of benzene in zeolites LTL and KL, as computed from 0.4 ns MD at 300 K using CVFF_AUG. Solid line: $G(\sigma)$ for all axes; dotted line: $G(\sigma)$ along *x*; dashed line: $G(\sigma)$ along *y*; long-dashed lines: $G(\sigma)$ along *z*, the channel axis.

extends to much higher wavenumbers: ≈60 cm^{-1}. In addition, there is a high frequency (HF) peak, at about ≈30 cm^{-1}, mostly originating in motions along *z*. We can generally separate external vibrations at a cation in two distinct parts: a vibration 'away from the cation', and a vibration 'parallel to the cation'. This has been observed, e.g. for methane [58] or oxygen in NaA [59], as well as for benzene in NaY [11,60] or in HY [61]. Since the peak at 30 cm^{-1} comes mainly from a contribution along *z*, the channel axis, it cannot be clearly attributed to the vibration 'away from the cation'. Rather, it is due to the geometry of the cage around the D cation site: in the vicinity of this site, benzene is constrained in the cage along *z*. The vibration 'away from the cation' appears only as part of the HF tail in the spectra along *x* and *y*.

All vibrations observed at infinite dilution are very low frequency ones, both in LTL and KL. It has been found for benzene in other zeolites, that the vibration 'away from the cation' is usually a HF one: up to 200 cm^{-1} for benzene in HY [61], and estimated from 50 to 100 cm^{-1} for benzene in NaY [11]. In KL, we do not observe any well-defined corresponding vibration, indicating a very flat potential. This flatness here is naturally related to the cation size, which becomes evident when comparing H^+, Na^+, and K^+.

Fig. 13 presents the evolution of the total vibrational density-of-states $G(\sigma)$ when the number of molecules increases. In LTL, $G(\sigma)$ at medium loading is very similar to that at low loading: indeed, we have seen that for two adsorbed molecules, they separate in different cages, so that each molecule feels an environment similar to infinite dilution. At high loading, there are two molecules per cage, so that the spectrum changes: most notably, a peak appears at higher frequency, that can be attributed to the correlated vibration of both benzene molecules together in the cage. Indeed, this peak can be seen also on $G(\sigma)$ computed for the COM of all atoms of the two benzene molecules together. In KL, putting two molecules in the same cage also shifts the peaks toward higher frequencies, for the same reason as in LTL. In contrast to LTL however, the spectrum at medium loading is similar to that for high loading, which reflects the presence of two benzene molecules in the same cage.

3.3. Self-diffusion coefficient

Getting a reliable diffusion coefficient from MD simulations is far from trivial. Indeed, a diffusion coefficient can only be measured in the long-time diffusive regime, thus requiring extremely long dynamics run, even for fast diffusion. Only in the last years have simulation duration reached the 20 ns or more required to sample a diffusivity of 10^{-10} m^2 s^{-1} [55,62]. Such long runs are necessary to observe the crossing of free energy barriers separating stable adsorption sites. Free energy sampling techniques can be used as an alternative to these long MD calculations, and this is an area of current active research [63,64].

A precise self-diffusion coefficient, however, is never more accurate than the underlying free energy landscape. In the absence of any exact energy functional, and since even experimental diffusion coefficients are estimated with a 50% error, it is doubtful whether such accuracy is of any use; rather, one needs

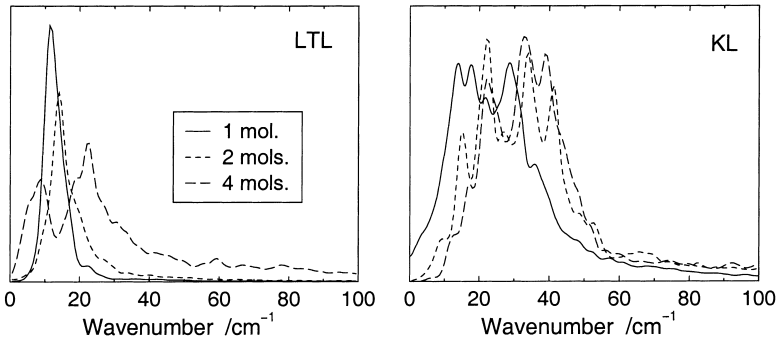

Fig. 13. Vibrational density-of-state $G(\sigma)$ for one to four molecules of benzene in two unit-cells of zeolites LTL and KL, as computed from 0.1 to 0.4 ns MD at 200 K using CVFF_AUG.

a reliable estimation of the uncertainty with which the self-diffusion coefficient is calculated. Defining the self-diffusion coefficient from the Einstein relation,

$$D = \frac{1}{6}\lim_{t\to\infty}\frac{1}{t}\langle \boldsymbol{r}^2(t)\rangle \tag{6}$$

it is usually estimated from the slope of the MSD versus time. One immediately sees that there are two competing aspects building the total uncertainty on D: (i) the limit $t \to \infty$ should correspond to a long enough time so that diffusive regime is reached, i.e. linear dependence of the MSD upon t; but (ii) the slope should be as near as possible from the origin to minimize the statistical uncertainty of the estimation. If the MD run is not long enough for a constant, far-ranging, beautifully linear regime to be observed, it is rather difficult to ascertain the total interval of confidence of the corresponding self-diffusion coefficient. It should also be noted that the MSD of any molecule in a periodically repeated cell is necessarily linear with t over lengths longer than the unit-cell; thus an observed hydrodynamic behavior can sometimes be an artifact of the simulation, especially with complex multi-molecule systems with strong molecule–molecule interactions, where coherence lengths can extend over more than one unit-cell.

Fortunately diffusion of adsorbed molecules in zeolites, as indicated in Section 1, follows most of the time a particularly simple process of site-to-site jumps by crossing free energy barriers. Therefore, one can define a 'basic diffusive event' corresponding to one of these jumps, delimiting the pausing time distribution in the stable site. Supposing that the pausing time distribution follows an exponential law corresponding to a random site-to-site process, we would have that

$$D = \frac{1}{6}\frac{a^2}{\tau} \tag{7}$$

where D indicates the self-diffusion coefficient, a the distance between two basic sites and τ the average residence time in the sites. This provides a direct measure of the uncertainty on D as:

$$\frac{\Delta D}{D} = \frac{\Delta\tau}{\tau} \tag{8}$$

$\Delta\tau$, for its part, is easily estimated from the simulation using the central limit theorem. In the general case, the pausing time distribution might not be exponential, so that Eq. (7) might not hold. We nevertheless suppose that Eq. (8) gives an estimate of the uncertainty on D. The residence time used to define uncertainties on the self-diffusion coefficient is in all cases the cage residence time, characterizing long-time transport, and not the cation residence time described in Fig. 11.

In the case of multiple molecules adsorbed in both KL and LTL, we could not define any self-diffusion coefficient from the simulations: indeed, only very few cage-to-cage jumps were observed in these cases, usually less than five, even in long runs. The reason for this behavior is of course both site blocking and benzene–benzene interactions, both tending to decrease the mobility of the adsorbed molecules. The arguments presented above, however, show that even if we had observed more jumps resulting in a well-defined self-diffusion coefficient, for medium and high loadings, the small size of the simulation cell along z could have artificially changed the site-to-site dynamics of the adsorbed molecules. Indeed, for two molecules adsorbed in LTL, where they tend to occupy different cages, we have observed correlated site-to-site jumps of both molecules; in the absence of a much longer dynamics on a much larger systems, there is however no way of deciding whether this correlation is an artifact of the simulation or a genuine phenomenon. For this reason, we will limit this discussion of the self-diffusion coefficient to infinite dilution alone.

Fig. 14 presents the MSD of benzene in LTL at infinite dilution for four temperatures, both in log–log and x–y plots. After an initial ballistic regime characterized by a slope of two on the log–log plot, we can observe some oscillations reflecting the confinement of the molecules in a cage, followed by the diffusive regime characterized by the slope of one. It is clear on the log–log plot that this diffusive regime does not persist for a very long time, and statistical uncertainties hide the linearity after as few as 50 ps, although the total MD simulation extended for 0.45 ns. On the x–y plot, we can derive from the linear regime the self-diffusion coefficient by limiting the regression under 100–200 Å^2, corresponding to a span of two to four unit-cells. This has been done for both LTL and KL, and the resulting self-diffusivities, are given in Fig. 15. The corresponding error bars are estimated from the

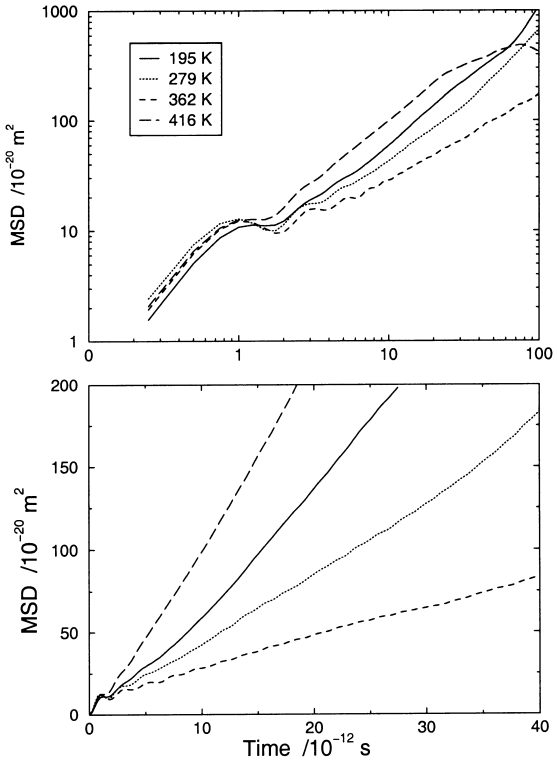

Fig. 14. Mean-square displacement of one molecule of benzene in zeolite LTL without compensating cations, as determined by a 0.4 ns MD run at various temperatures using CVFF_AUG. The top graph presents a log–log plot, the bottom one the corresponding *x*–*y* graph.

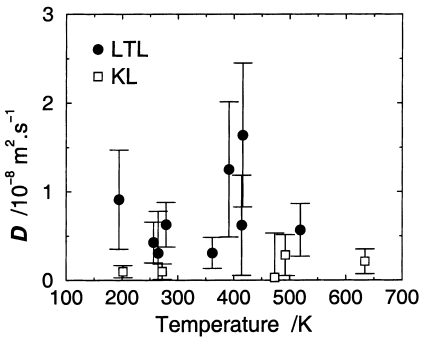

Fig. 15. Self-diffusion coefficient of a single benzene molecule in zeolites LTL and KL, as determined from a 0.4 ns MD run using CVFF_AUG. Error bars give the 95% confidence interval, estimated using the procedure indicated in the text.

site residence times, using a student *t*-distribution with a 95% confidence interval.

One immediately sees why it is so important here to estimate reliably the confidence interval: indeed, the temperature dependence of the diffusion coefficient appears to be rather strange, compared with the usual exponential dependence observed for diffusion of guest molecules in zeolites [65]. In particular, the self-diffusion of benzene in LTL behaves clearly non-monotonically with a minimum of around 300–350 K and an increase at higher temperatures. In KL, *D* remains much smaller, but the statistical uncertainties due to very sparse cage-to-cage jumps make it difficult to really quantify its temperature dependence; it appears to be much smaller than the 0 K energy barrier found from constrained minimization, i.e. 34 kJ mol^{-1}. This behavior clearly demonstrates the entropic nature of the diffusion process of benzene in this zeolite, which we noted in Section 3.2 when discussing the free energy barriers.

3.4. Energy versus entropy

In this section, we would like to compare the results from static and dynamic calculations on benzene in zeolite L with and without compensating K^+ cations, as given in the above subsections. As a general rule, static studies focus on the energetics of the system, while dynamic studies probe its entropic dependence. The interest of studying benzene both in LTL and KL lies in the fact that entropic effects due to confinement are similar for both systems, while energetics is much stronger in KL due to the cation–benzene interaction. The results presented here can be summarized by the following comments.

The competing effects of energy and entropy are quite apparent in this study: energy tends to localize adsorption, and entropy to delocalize it; energy tends to cluster benzene molecules in the same cage, entropy to spread them in different cages; energy stabilizes the 12T window site in KL, while entropy destabilizes it. Entropic effects are clearly preponderant in LTL, already at 200 K: the clearest view might be given by the temperature dependence of the self-diffusion coefficient, which does not follow anything approaching Arrhenius behavior. It is indeed known that entropy plays an important role in all-siliceous zeolites [3,4].

In KL, the picture is more contrasted, as the control of the adsorbate's dynamics shifts from energy to entropy as the temperature increases between 200 and 600 K. This is clearly apparent on the temperature dependence of the K-benzene or benzene–benzene pair distribution functions. However even at low temperature, entropic effects are not negligible, for example, we do not observe any adsorption on the KL 12T window, which is predicted by constrained energy minimization results. This is in accordance with IR measurements [31].

The clear conclusion of this study is, not to rely uniquely on simple energetic simulations alone: while energy plays an important part in zeolite, for temperatures of interest in experimental set-ups, entropy also plays an important role. Of course this conclusion is not completely general, as the importance of energetics depends on the particular system of interest, as well as the potentials. Furthermore, entropic effects themselves depend on the structure of the zeolite and adsorbate. For example, we have shown in a study of benzene in NaY that even at high temperature energetics remains preponderant [3]. Considering the forcefields used, which are representative of the type of forcefields generally considered for adsorbates in zeolites, it is clear that adsorption on a cation will be stronger as the radius of this cation decreases. In the first part of this study, we have shown that the radius of the K^+ is probably slightly overestimated by CVFF_AUG, which therefore probably minimizes the influence of energy. This does not change the conclusions presented here but shifts up the temperature for which entropic effects might become preponderant over energetic effects. By estimating free energy barriers to diffusion of benzene in KL and LTL, we have quantified entropic effects for these systems between 200 and 600 K, the entropic part of the barrier amounts to $\approx 0.02\,\mathrm{kJ\,mol^{-1}\,K^{-1}}$, which is about $6\,\mathrm{kJ\,mol^{-1}}$ at 300 K. This value is rarely negligible, except for very high energy barriers to the diffusion.

We have also shown that the entropic barrier is similar at infinite dilution for both KL and LTL, showing that it should be possible to estimate the order of magnitude of entropic effects by a simpler study of diffusion in the all-siliceous zeolite. However, this does not remain valid when loading increases.

4. Conclusion

We have used a number of standard forcefield-based molecular simulation techniques available within the commercial InsightII and Cerius^2 packages of MSI to determine and validate a model of zeolite L, with and without compensating potassium cations KL and LTL, respectively, and to study the adsorption and dynamics of benzene adsorbed in this structure. We have focused on the differences between KL and LTL by systematically running the same simulations in the two structures. We have used static simulation techniques involving only energy minimization to determine the minimum energy sites at 0 K, and the MEP between these sites. We have also used short (100–500 ps) MD simulations at different temperatures and loadings to determine the influence of entropic effects on the dynamics of benzene in zeolite L.

The model zeolite KL (Si/Al = 3.0) we constructed is based on neutron diffraction data of Newsam [25]. Four different configurations of the Al atoms were initially considered. K^+ cations were introduced in the structure, using the cation-locator package available within the Cerius^2 environment. The resulting distribution of the cations matched exactly the neutron diffraction data [25]: the four resulting models only differed in the local arrangement of the K^+ cations at a D site in the supercage. Simulated IR and XRD spectra for all four models were also identical, so that we arbitrarily chose one of these models to study the diffusion of benzene. This model was minimized using the Burchart-UFF forcefield, also available in MSI's Cerius^2 package. A comparison of the IR and XRD spectra with experimental data showed that this forcefield reproduces well both the structure and dynamics of KL. The commonly used forcefield derived by van Beest et al. [38] also gave good results, as did the average T-site forcefields of Auerbach et al. [13]. On the other hand, the bare UFF forcefield, which was not parametrized for zeolites, led to a poor agreement with both of the structure and of the dynamics of the KL framework.

The model zeolites KL and LTL were kept fixed to study the adsorption and dynamics of benzene. We focused on comparing the results of static simulation methods, i.e. solid-docking, packing, and solid-diffusion, available within the InsightII environment of MSI, using energy minimization alone,

and MD, using Discover3, also from MSI. These are standard simulation methods and packages, routinely used to estimate the efficiency of zeolites as molecular sieves. Solid-docking and packing packages were employed to determine the minimum energy sites for benzene in LTL and KL, solid-diffusion to estimate the MEP between these sites, and Discover3 to study the dynamics of benzene in LTL and KL between 200 and 600 K, at infinite dilution, one molecule per unit-cell, and two molecules per unit-cell. All benzene–zeolite interactions were computed with the CVFF_AUG forcefield, also from MSI.

Docking and packing studies show that benzene in both LTL and KL is preferentially adsorbed inside the supercage. In KL, the preferred adsorption site is next to a K(D) cation inside the supercage. The 12T window is a local minimum in KL but not in LTL, probably due to the slight difference in size: 10.7 Å from O to O in KL, against 10.4 in LTL. This window site seems favored as the number of adsorbed benzene increases. Energy barriers to the diffusion at infinite dilution are estimated to 7.5 kJ mol^{-1} in LTL, and about 34 kJ mol^{-1} in KL.

Entropic effects however have a strong influence on the adsorption behavior of benzene, as the results obtained from MD simulation are very different from the static simulations: energy tends to localize adsorption of benzene in KL next to a K^+ cation, entropy to delocalize it over the whole cage; energy tends to favor the 12T window site in KL, while entropy makes this site no longer stable, for all loadings and temperatures studied; energy tends to cluster up to three benzene molecules in the same cage, entropy to separate them in different cages. We can estimate an order of magnitude of the entropy barrier to the diffusion from a linear fit of the potential of MF along the channel axis with temperature: it amounts to $\approx$0.02 kJ mol^{-1} K^{-1} at infinite dilution, both for KL and LTL. Even if the energy part of the interaction between benzene and KL is underestimated, which is likely from the overestimation of the K^+ radius, this would amount to about 6 kJ mol^{-1} at 300 K, which is not negligible except for very high energy barriers.

Our MD simulations agree with IR measurements in that the 12T window site appears not to be an adsorption site, whatever the temperature and loading [31,32]. The nature of the adsorption site, i.e. benzene 'capping' a K^+ cation at a D site, also agrees well with experimental data [25]. More importantly, benzene pausing time at a cation site in KL was determined by Sato et al. [30] using ^{2}H NMR to be about six orders of magnitude larger than what is estimated from the simulation. One reason for both results might be that the radius of the K^+ ion is overestimated by CVFF_AUG: if one is interested in exact agreement between experiment and simulation, a reparametrization of the corresponding interaction parameters is probably required. However, we feel this would not change our conclusions on the influence of entropy on adsorption and diffusion of benzene in LTL and KL, but only the temperature for which entropic effects would become preponderant over energetics. Indeed, the fact that the estimated ΔS in KL is very similar to that in LTL suggests that entropic effects are mainly due to the geometry of the channel, rather than to the compensating cations.

The last observation leads to an important conclusion; indeed, it should be possible to estimate entropic barriers to diffusion of a given molecule in a particular zeolite from a study of the diffusion in the all-siliceous equivalent of this zeolite, which is much less computationally intensive. This argument forms the basis of most simulations of diffusion in all-siliceous equivalent to active zeolites [8]. We find here that, although completely justified at infinite dilution, this argument does not remain valid at finite loading: the influence of intermolecular interactions at medium loading is very different in LTL, where entropic effects win and molecules tend to separate in different cages, and KL, where for not-too-high temperatures energy wins and molecules cluster in the same cage.

Acknowledgements

All authors wish to thank the FUNDP for the use of the SCF Center, a joint project between the FNRS, IBM Belgium, and the FUNDP. They acknowledge MSI for the use of their software in the framework of the 'catalysis and sorption' consortium, and especially Dr. J.M. Newsam for fruitful 'electronic' discussions. They also thank Professor B.L. Su and Dr. J.-L. Blin, from the Laboratoire de Chimie des Matériaux Inorganiques at the FUNDP, for the experimental spectra of KL. F.J. is pleased to acknowledge A.A. Lucas, Director of the PAI 4-10, for the attribution of a post-doctoral fellowship.

References

[1] M. Bülow, A. Micke, Adsorption 1 (1995) 29.
[2] E.G. Derouane, J. Mol. Catal. A: Chem. 134 (1998) 29.
[3] F. Jousse, L. Leherte, D.P. Vercauteren, J. Phys. Chem. B 101 (1997) 4717.
[4] R. Krishna, B. Smit, T.J.H. Vlugt, J. Phys. Chem. A 102 (1998) 7727.
[5] T.J.H. Vlugt, R. Krishna, B. Smit, J. Phys. Chem. B 103 (1999) 1102.
[6] P. Demontis, S. Yashonath, M.L. Klein, J. Phys. Chem. 93 (1989) 5016.
[7] E. Cohen de Lara, R. Kahn, A.M. Goulay, J. Chem. Phys. 90 (1989) 7482.
[8] P. Demontis, G.B. Suffritti, Chem. Rev. 97 (1997) 2845.
[9] S. Fritzsche, R. Haberlandt, J. Kärger, H. Pfeifer, H. Heinzinger, M. Wolfsberg, Chem. Phys. Lett. 242 (1995) 361.
[10] D.A. Faux, J. Phys. Chem. B 102 (1998) 10658.
[11] F. Jousse, S.M. Auerbach, J. Chem. Phys. 107 (1997) 9629.
[12] D.I. Kopelevich, H.-C. Chang, Phys. Rev. Lett. 83 (1999) 1590.
[13] S.M. Auerbach, N.J. Henson, A.K. Cheetham, H.I. Metiu, J. Phys. Chem. 99 (1995) 10600.
[14] Cerius^2 3.0 Modeling Environment, MSI, San Diego, 1997.
[15] InsightII 4.0.0 User Guide, MSI, San Diego, 1996.
[16] E.G. Derouane, J.-M. André, A.A. Lucas, J. Catal. 110 (1988) 58.
[17] I. Derycke, J.-P. Vigneron, Ph. Lambin, A.A. Lucas, E.G. Derouane, J. Chem. Phys. 94 (1991) 4620.
[18] P. Santikary, S. Yashonath, J. Phys. Chem. 98 (1994) 9252.
[19] S. Yashonath, S. Bondyopadhyay, Chem. Phys. Lett. 228 (1994) 284.
[20] M. Ghosh, G. Ananthakrishna, S. Yashonath, P. Demontis, G. Suffritti, J. Phys. Chem. 98 (1994) 9354.
[21] C. Rajappa, S. Yashonath, J. Chem. Phys. 110 (1999) 5960.
[22] R.E. Jentoft, M. Tsapatsis, M.E. Davis, B.C. Gates, J. Catal. 179 (1998) 565.
[23] J.M. Newsam, B.G. Silbernagel, A.R. Garcia, R. Hulme, J. Chem. Soc., Chem. Commun. 664 (1987).
[24] E.G. Derouane, D.J. Vanderveken, Appl. Catal. 45 (1988) L15.
[25] J.M. Newsam, J. Phys. Chem. 93 (1989) 7689.
[26] B.G. Silbernagel, A.R. Garcia, J.M. Newsam, R. Hulme, J. Phys. Chem. 93 (1989) 6506.
[27] B.L. Su, D. Barthomeuf, Zeolites 15 (1995) 470.
[28] B.L. Su, D. Barthomeuf, Appl. Catal. A: Gen. 124 (1995) 81.
[29] B.L. Su, Zeolites 16 (1996) 75.
[30] T. Sato, K. Kunimori, S. Hayashi, Phys. Chem. Chem. Phys. 1 (1999) 3839.
[31] B.L. Su, V. Norberg, C. Hansenne, Langmuir 16 (2000) 1132.
[32] B.L. Su, V. Norberg, C. Hansenne, A. de Mallmann, Adsorption 6 (2000) 61.
[33] N.J. Henson, A.K. Cheetham, B.K. Peterson, S.D. Pickett, J.M. Thomas, J. Comput.-Aided Mater. Design 1 (1993) 41.
[34] R.C. Deka, R. Vetrivel, J. Catal. 174 (1998) 88.
[35] D.W. Breck, Zeolite Molecular Sieves, Wiley, New York, 1974.
[36] Forcefield-Based Simulations, MSI, San Diego, 1997, p. 38.
[37] E. de Vos Burchart, V.A. Verheij, N. van Bekkum, B. van de Graaf, Zeolites 12 (1992) 183.
[38] B.W.H. van Beest, G.J. Kramer, R.A. van Santen, Phys. Rev. B 64 (1990) 1955.
[39] G.J. Kramer, N.P. Farragher, B.W.H. van Beest, R.A. van Santen, Phys. Rev. B 43 (1991) 5068.
[40] N.J. Henson, A.K. Cheetham, A. Redondo, S.M. Levine, J.M. Thomas, in: J. Weitkamp, H.G. Karge, H. Pfeifer, W. Hölderich (Eds.), Zeolites and Related Microporous Materials: State of the Art 1994, Elsevier, Amsterdam, 1994, pp. 2059–2066.
[41] J.M. Newsam, C.M. Freeman, A.M. Gorman, B. Vessal, J. Chem. Soc., Chem. Commun. 1945 (1996).
[42] N.J. Henson, S.M. Auerbach, DIZZY Computational Chemistry Program, Materials Department, University of California, Amherst, 1994–1998.
[43] R.M. Barrer, H.Z. Villiger, Kristallogr. Kristallgeom. Kristallphys. Kristallchem. 128 (1969) 352.
[44] M.P. Allen, D.J. Tildesley, Computer Simulations of Liquids, Clarendon Press, Oxford, 1987.
[45] D. Frenkel, B. Smit, Understanding Molecular Simulations, Academic Press, San Diego, 1996.
[46] F. Jousse, L. Leherte, D.P. Vercauteren, J. Mol. Catal. A: Chem. 119 (1997) 165.
[47] L.M. Bull, N.J. Henson, A.K. Cheetham, J.M. Newsam, S.J. Heyes, J. Phys. Chem. 97 (1993) 11776.
[48] P.J. O'Malley, C.J. Braithwaite, Zeolites 15 (1995) 198.
[49] F. Jousse, D.P. Vercauteren, S.M. Auerbach, J. Phys. Chem. B 104 (2000) 8768.
[50] L.R. June, A.T. Bell, D.N. Theodorou, J. Phys. Chem. 96 (1992) 1051.
[51] E. Hernandez, C.R.A. Catlow, Proc. R. Soc. London A 448 (1995) 143.
[52] T. Mosell, G. Schrimpf, C. Hahn, J. Brickmann, J. Phys. Chem. 100 (1996) 4571.
[53] G. Sastre, N. Raj, C.R.A. Catlow, R. Roque-Malherbe, A. Corma, J. Phys. Chem. B 102 (1998) 3198.
[54] A. Bouyermaouen, A. Bellemans, J. Chem. Phys. 108 (1998) 2170.
[55] L.N. Gergidis, D.N. Theodorou, J. Phys. Chem. B 103 (1999) 3380.
[56] X. Shi, L. Bartell, J. Phys. Chem. 92 (1988) 5667.
[57] P. Hobza, H.L. Setzle, E.W. Schlag, J. Phys. Chem. 100 (1996) 18790.
[58] R. Kahn, E. Mouche, E. Cohen de Lara, J. Chem. Soc., Faraday Trans. 86 (1990) 1905.
[59] F. Jousse, A.V. Larin, E. Cohen De Lara, J. Phys. Chem. 100 (1996) 238.
[60] H. Jobic, A.N. Fitch, in: H. Chon, S.-K. Ihm, Y.S. Uh (Eds.), Studies on Surface Science Catalysis, Vol. 105, Elsevier, Amsterdam, 1997, pp. 559–566.
[61] F. Jousse, S.M. Auerbach, D.P. Vercauteren, J. Phys. Chem. B 104 (2000) 2360.
[62] E.B. Webb III, G.S. Grest, Catal. Lett. 56 (1998) 95.
[63] A.F. Voter, J. Chem. Phys. 106 (1997) 4665.
[64] G. Besold, J. Risbo, O.G. Mouritsen, Comp. Mater. Sci. 15 (1999) 311.
[65] J. Kärger, Phys. Rev. A 45 (1992) 4173.